Biodegradable Nanocomposites of Cellulose Acetate Phthalate and Chitosan Reinforced with Functionalized Nanoclay: Mechanical, Thermal, and Biodegradability Studies

Aashish Gaurav,[1] A. Ashamol,[2] M. V. Deepthi,[2] R. R. N. Sailaja[2]

[1]*Deparment of Chemical Engineering, IIT, Kharagpur, West Bengal, India*
[2]*The Energy and Resources Institute, Bangalore 560071, Karnataka, India*

Received 16 December 2010; accepted 20 July 2011
DOI 10.1002/app.35591
Published online 19 December 2011 in Wiley Online Library (wileyonlinelibrary.com).

ABSTRACT: Biodegradable nanocomposites of **c**ellulose acetate phthalate and **c**hitosan reinforced with functionalized nanoclay (NC) were prepared. The **NC** loading was varied from 0 to 10%. The mechanical and thermal properties have been investigated for these composites. The nanocomposites exhibited enhanced mechanical properties due to the addition of **NC**. The scanning electron micrographs of the blend specimens also support the above observations. Thermogravimetric analyses were carried out to assess the degradation stability of the blends. The blend shows an increase in the rate of biodegradation and water uptake with higher loading of **NC**. The exfoliation of **NC** was analyzed by X-**r**ay diffraction studies. © 2011 Wiley Periodicals, Inc. J Appl Polym Sci 125: E16–E26, 2012

Key words: cellulose acetate phthalate; chitosan; nanoclay; mechanical and thermal properties; biodegradability

INTRODUCTION

The development of high performance bioplastics is gaining prominence owing to increasing plastic pollution and also to conserve the diminishing global petroleum reserves. Further, biopolymers are inexpensive, renewable, and sustainable alternatives, which can replace petrochemical-derived synthetic polymers. Cellulose and chitosan are among the most abundant natural biopolymers, which are inexpensive, renewable, and biodegradable with antibacterial properties.

Biobased nanocomposites are produced in which atleast one component is nanosized and acts as a reinforcement even with low content.[1] Thus, chitosan reinforced with nanosized cellulose whiskers, which have been reported to exhibit improved tensile and water resistance.[2] El-Tahlawy et al.[3] developed spinnable esterified chitosan butyrate/cellulose acetate blend fibers with enhanced properties. Films of iminochitosan with cellulose acetate yielded smooth homogeneous films[4] with good mechanical strength.

In this study, an esterified cellulose derivative has been blended with chitosan and reinforced with surface functionalized nanoclay (NC). The mechanical, thermal, and biodegradability characteristics have been investigated. It has been found earlier that interactions do exist between chitosan and cellulose as reported by Hasegawa et al.[5] An interpenetrating polymer network forms between cellulose and chitosan with decreasing crystallinity as chitosan loading is increased as reported by Cai and Kim[6] An increased thermal stability of chitosan-montmorillonite biocomposite films dependent of clay content was reported by Altinisik et al.[7] Miscibility studies of chitosan blend with cellulose ethers revealed that the blends are partially miscible in dry state although, hydrogen bonding exists between the functionalized groups.[8] However, cellulose acetate/chitosan blend films have been found to have improved miscibility and good mechanical properties as studied by Liu and Bai.[9] Similar studies were also reported by Shih et al.[10] Clay reinforced cellulose acetate nanocomposites show an improvement in mechanical properties and thermal stability.[11] In this article, the effect of adding NC to a blend of cellulose acetate phthalate (CAP) and chitosan has been investigated. The NC used is surface modified to enhance dispersion and bonding with the blend components.

EXPERIMENTAL

Materials

CAP (degree of substitution for acetyl and phthalyl groups are 1.07 and 0.77, respectively) with

Correspondence to: R. R. N. Sailaja (rrnsb19@rediffmail.com).

molecular weight 2534.12 was purchased from GM Chemicals, Mumbai. Chitosan (with 85% deacetylation and molecular weight ranging from 10,000 to 15,ooo) was purchased from Marine chemicals, Cochin, Kerala. Silane-treated NC was obtained from Sigma Aldrich (USA). Glycerol and other common solvents were obtained from S.D. Fine Chem, Mumbai.

Preparation of blend

A total of 100 g mixture of CAP (60 g) and chitosan (40 g) powders were taken for the preparation of composites. NC quantity was varied from 0 to 10 wt %. The mixture was mixed in a kitchen mixer for 10 min. Glycerol (40% of the weight of the mixture) was added to the mixture and then sonicated using Ultra sonicator (Branson, 2510E/DTH) for 30 min. Water (100 mL) was then added to the mixture and the contents were kneaded to form a dough. The blend of pure CAP and chitosan without NC also contained the same amount of glycerol and water. The dough samples were kept in zip-locked plastic packets in refrigerator for further processing.

Compression molding

The dough was partially dried prior to compression molding. The semi-dried blend was placed in a mold covered with two polished stainless steel plates and then compression molded using a locally fabricated hot press. Sheets were molded at 130°C under a pressure of 15 MPa for 3 min, and then cooled to about 50°C for 15 min under constant pressure before releasing the pressure for demolding. The sheets were then cut into rectangular strips and these strips were subjected to mechanical testing.

Mechanical properties of the blend

Tensile properties

The tensile properties of the blends were measured by Zwick UTM (Zwick Roell, ZHU, 2.5) with Instron tensile flat surface grips at a crosshead speed of 2 mm/min. The tensile tests were performed as per ASTM D 638 method. The specimens tested were of rectangular shape having length, width, and thickness of 7, 1.5, and 0.3 cm, respectively. A minimum of five specimens were tested for each variation in composition of the blend and results were averaged. Predictive theoretical models have been used to analyze the observed experimental results.

Flexural properties

The flexural properties of the blends were measured by Zwick UTM (Zwick Roell, ZHU, 2.5) with a preload speed of 10 mm/min. The tests were performed as per ASTM D 790-03 method. The samples were having a length of 5 cm, width of 2 cm, and a thickness of 0.3 cm. A minimum of five specimens were tested for each blend and the results were averaged.

Compressive properties

The compressive properties of pure CAP, pure chitosan, and the blends were performed as per ASTM D 695 by Zwick UTM (Zwick Roell, ZHU, 2.5) with a preload of 4.5 k*N* and a test speed of 3 mm/min. The samples were having a length of 3 cm, width of 2 cm, and a thickness of 0.3 cm. A minimum of five specimens were tested for each composition and the results were averaged.

Thermal analysis

Thermogravimetric analysis (TGA) was carried out for the blends using Perkin-Elmer Pyris Diamond 6000 analyzer in nitrogen atmosphere. The samples were subjected to a heating rate of 10^0C/min in the heating range of 40–600°C using Al_2O_3 as the reference material.

Differential scanning calorimetry (DSC) of the nanocomposite specimens have been performed in a Mettler Toledo instrument (model DSC 822e; Mettler Toledo AG, Switzerland). Samples are placed in sealed aluminum cells, with a quantity of less than 10 mg and scanning at a heating rate of 10°C/min up to 250°C.

FTIR spectroscopy

Fourier transform infrared spectroscopy (FTIR; Perkin-Elmer spectrum 1000) analysis for the Pure CAP, chitosan, and the nanocomposites was performed.

X-ray diffraction

XRD measurements for the nanocomposites have been performed using advanced diffractometer (PANalytical, XPERT-PRO) equipped with a Cu-kα radiation source ($X = 0.154$ mm). The diffraction data were collected in the 2θ range of 3–30° using a fixed-time mode with a step interval of 0.05°.

Blend morphology

Scanning electron microscopy (SEM; LEICA.S440, Model 7060) is used to study the morphology of the fractured and unfractured specimens. The specimens are gold sputtered prior to microscopy. The SEM morphology of the unfractured blend specimens was taken after soaking the samples in dilute sulfuric

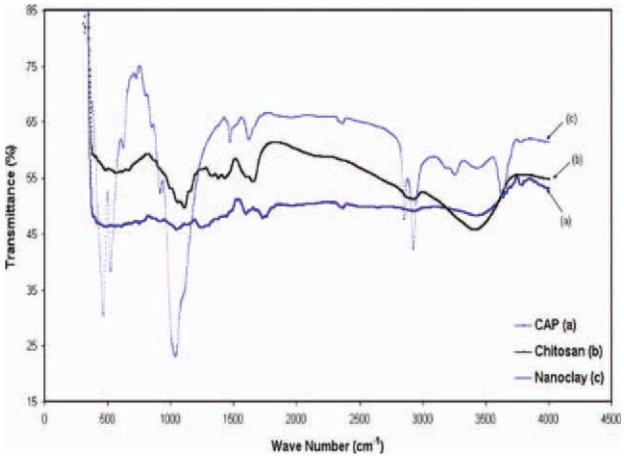

Figure 1 FTIR Spectra of pure cellulose acetate phthalate, chitosan, and silanated nanoclay. [Color figure can be viewed in the online issue, which is available at wileyonlinelibrary.com.]

acid for 24 h and then drying in air after thoroughly rinsing it in distilled water.

Water absorption

Water absorption index of the samples were measured according to ASTM D 570-81 with minor modification.[12] The dried sample is weighed and submerged in distilled water at room temperature for 24 h. The extra water on the surface of the specimen after soaking is removed by placing it in an air oven at 50°C and the specimen were weighed again. The container without the soaking specimen is placed in an air oven at 50°C for 72 h to evaporate the water, and the water-soluble content obtained was equal to the increase in container weight. The absorption (AB) is then calculated by the following eq. (1):

$$\mathrm{AB} = (W_1 - W_o + W_{\mathrm{sol}})/W_o \qquad (1)$$

where W_1, W_o, and W_{sol} are the weight of the specimen containing water, the weight of the dried specimen, and the weight of the water-soluble residues, respectively.

Biodegradation

The biodegradation of the blend specimens were carried out by soil burial method.[13] Soil-based compost was taken in small chambers. Humidity of the chambers was maintained at 40–45% by sprinkling water. The chamber were stored at 30–35°C. Rectangular specimens were buried completely into the wet soil at a depth of 10 cm. Samples were removed from the soil at constant time intervals (15 days) and washed gently with distilled water and dried in vacuum oven at 50°C to constant weight. Weight loss percentages of the samples with respect to time were recorded to determine the extent of biodegradation.

RESULTS AND DISCUSSIONS

Bionanocomposites of CAP and chitosan have been prepared and characterized using FTIR, XRD, and SEM. The mechanical and thermal properties of the nanocomposites have also been studied.

FTIR spectroscopy

Figure 1 shows the FTIR spectroscopy of neat chitosan, CAP, and NC, while that of CAP–chitosan nanocomposites are shown in the Figure 2. Spectroscopy of neat chitosan, CAP, and NC are given for the sake of comparison. The blends with 0% NC does not have the peak at 1643 cm^{-1}, which is a characteristic of amide I band. This is mainly attributed to the fact that the amide group of chitosan has reacted with the carboxyl group of CAP. Silanated-NC has two main peaks. The first one is at 1025 cm^{-1} [14] for the Si–O-stretching of silicate present and also of the interaction with platelet surface. The second peak is at 1603 cm^{-1} for $-NH_2$ (primary amine) stretching, which does not appear for the blends. The characteristic bands for CAP at 1035, 1239, 1589, 1724, and 2913 cm^{-1} are respectively for –C–O– stretching, –C–O–C– stretching, –C=C– conjugated vinyl aromatic ring, –C=O carboxyl group, and asymmetric and symmetric stretching of methyl –C–H groups.[15] All the above bands are also seen in the blends. However, the other bands overlap with that of CAP and chitosan.

Stress–strain curves

The engineering stress–strain curves for CAP–chitosan nanoblends are shown in Figure 3. The stress–strain curves for neat CAP and chitosan are also given in the figure for comparison. CAP [curve (a)] is

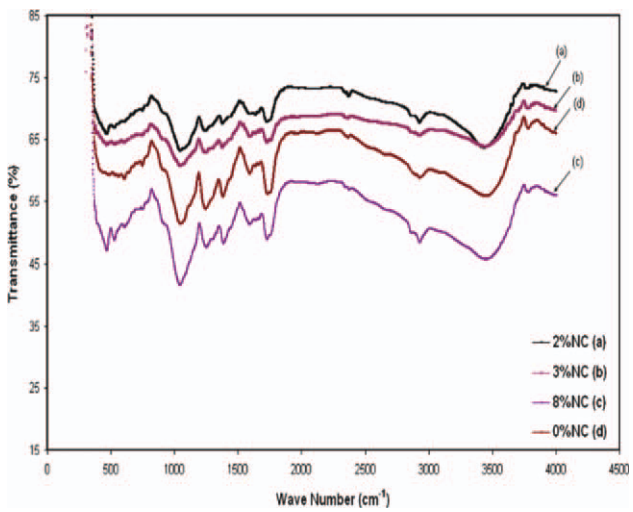

Figure 2 FTIR Spectra of CAP–chitosan–nanoclay blends. [Color figure can be viewed in the online issue, which is available at wileyonlinelibrary.com.]

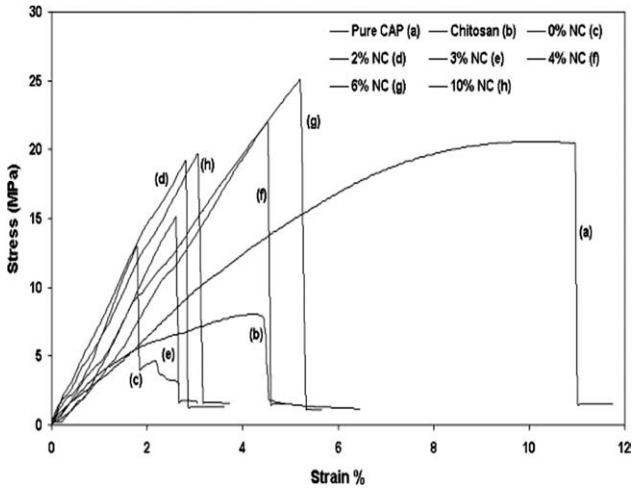

Figure 3 Plots of engineering stress–strain curves for pure cellulose acetate phthalate, chitosan, and CAP–chitosan–nanoclay blends.

more ductile when compared with chitosan [curve (b)], which has poor stress resistance and has brittle characteristics. The blend, however [curve (c)], exhibits higher stress value when compared with either of the blend components. Addition of NC [curve (d)–(f)] improves both stress as well as strain values owing to its reinforcing effect among the blend components.

The optimal stress values at 6% NC [curve (g)] shows, values higher than either CAP or chitosan with a strain values higher than that of chitosan. However, higher loading of NC of 10% [curve (h)] has a detrimental effect on the mechanical properties of the blend. This may be due to saturation of reactive sites of CAP or chitosan, which can react with the amine group of silane-treated NC. Thus, excess NC behaves like a separate third phase, which reduces the properties.

Effect of NC addition on mechanical properties

Tensile properties

Figure 4 shows the plot of relative tensile properties (i.e., relative to blend without NC) versus volume fraction of NC (ϕ). The relative elongation at break (REB) increases by adding NC up to $\phi = 1.0147$ (i.e., 6% NC) and reaches an optimal value of 1.8. This is contrary to the expectation that the addition of rigid NC particles had to lower the REB values and, in this case, the elongation at break values are even higher than either CAP or chitosan. A similar observation was made by Balakrishnan et al.[16]. Sue et al.[17] also did not observe a lowering in strain by adding rigid zirconium phosphate particles, although the mechanism is not well understood. It may be due to the fact that the amine group of silane-treated NC gets coated/interacted with CAP and the plastic deformation gets initiated around the blend particles. CAP is relatively more ductile than chitosan and NC, and this also helps in further anchoring the two blend components.

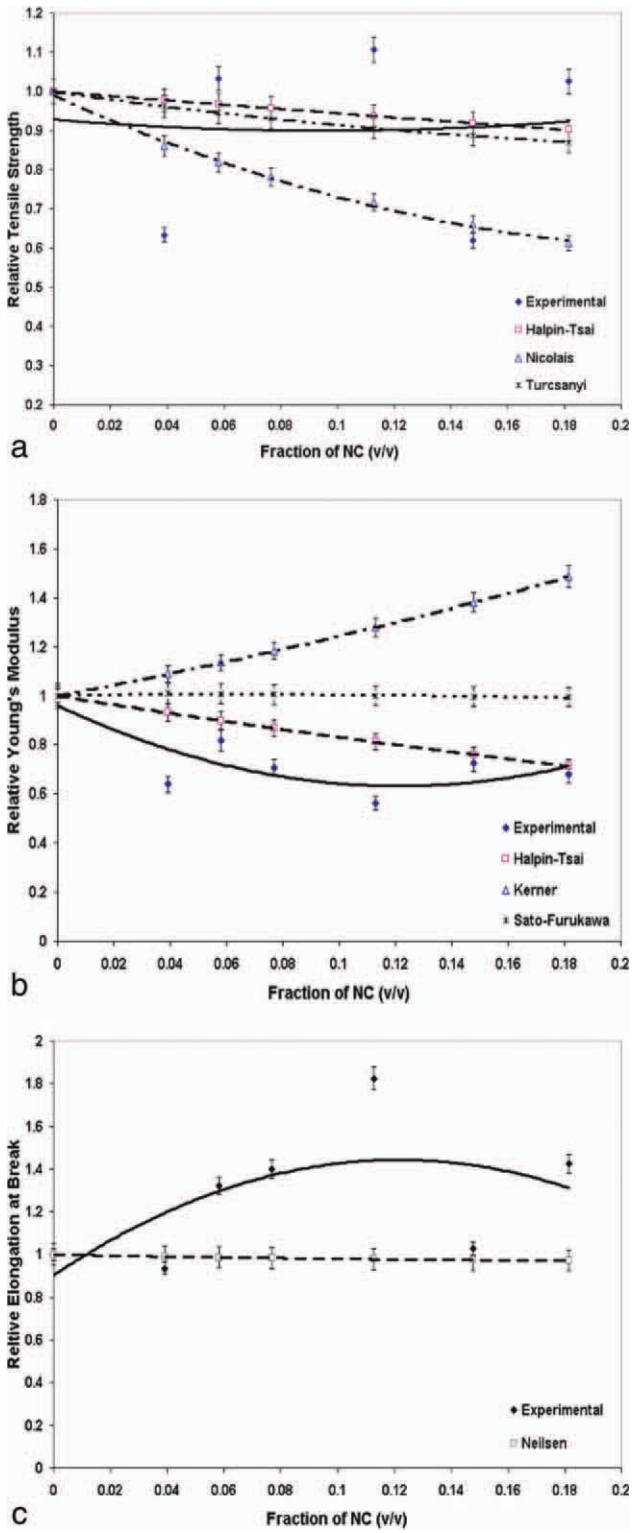

Figure 4 Plots of relative tensile properties versus volume fraction of nanoclay. (a) Relative tensile strength, (b) relative Young's modulus, (c) relative elongation at break. [Color figure can be viewed in the online issue, which is available at wileyonlinelibrary.com.]

The relative tensile strength (RTS) of the nanocomposites also showed a 10% increase when compared with blends without NC. The optimal value is reached at $\phi = 1.0147$ (i.e., 6% NC loading) beyond, which it is detrimental for the nanoblends. It may be due to the fact that all the reactive sites have been used up to this NC loading and with further NC loading, they agglomerate due to the presence of excess unreacted sites.

The relative tensile modulus (RYM) values also reduce due to the addition of NC and the curve is a mirror image of that obtained for REB, although in most cases, the addition of rigid particles such as starch to a ductile matrix exhibits an increase in modulus.[18]

To further analyze the obtained experimental results, the following predictive theories have been used as described below.

Figure 4(a) shows the plot of RTS values versus volume fraction of NC (ϕ). The volume fraction of NC, was calculated using the following eq. (2):

$$\phi_i = \frac{(w_i/\rho_i)}{\sum (w_i/\rho_i)} \tag{2}$$

In eq. (2) w_i and ρ_i is the weight fraction and density of component i in the blend. The density values of CAP, chitosan, and NC have been measured to be 0.92, 0.54, and 0.36 g/cm^3, respectively.

Three models were used to compare the obtained experimental tensile strength values. The first is the Nicolais and Narkis model,[19] which is as follows.

$$\text{RTS} = \frac{\sigma_b}{\sigma_o} = 1 - 1.21\phi^{2/3} \tag{3}$$

In eq. (3), σ_b and σ_O are the tensile strength of the nanoblends and tensile strength of the blend without NC reinforcement. The model assumes that addition of filler reduces the effective cross-sectional area and there exists no adhesion between filler and matrix. As observed in plot 4(a), the theoretical values of eq. (3) and the experimental RTS values does not match.

The second model is the Halpin–Tsai model,[19] which is given below in eq. (4)

$$\text{RTS} = \frac{\sigma_b}{\sigma_o} = \frac{1 + G\eta_T\phi}{1 - \eta_T\phi} \tag{4}$$

In eq. (4), η_T is given by the following equation.

$$\eta_T = \frac{R_T - 1}{R_T + G} \text{ and } G = \frac{7 - 5\upsilon}{8 - 10\upsilon} \tag{5}$$

In eq. (5), R_T is the ratio of tensile strength of NC to the tensile strength of CAP/chitosan blend without NC. R_T was determined by trial and error by minimizing the difference between the obtained experimental results and calculated theoretical values, this was found to be 0.548. υ is the Poisson's ratio of CAP/chitosan blend, which is taken to be 0.37.[20] The predicted values obtained from eq. (5) are closer to the experimental values when compared with that obtained by Nicolais–Narkis model, as the Halpin–Tsai model assumes good adhesion between the blend components.

The third model is the Turcsanyi model,[21] which includes an interfacial parameter B, which is a measure of extent of adhesion of the filler with the matrix and the equation, is given below as follows.

$$\text{RTS} = \frac{\sigma_b}{\sigma_o} = \frac{1 - \phi}{1 + 2.5\phi}\exp(B\phi) \tag{6}$$

The value of B was determined to match with the experimental results and this was found to be 2.4, which indicates good adhesion. The amine group of silane on NC interacts well with the blend components and thus leads to enhanced tensile strength values. A similar analysis using the above model was carried out by Zou et al.[22] for polyesteramide composites with different fillers. Thus, blends with poor tensile strength showed a B value of 0.25 (no adhesion), while higher values (e.g., 3.44 for talc) indicated better adhesion. The values obtained for eq. (6) are also shown in Figure 4(a). The predicted values of the Turcsanyi model are higher than that obtained for eq. (3), but theoretical values obtained from Halpin–Tsai model are closer to the experimental data.

Figure 4(b) shows a plot of relative tensile modulus (RYM) versus volume fraction of NC. The RYM values reduce with the increase in NC content as described earlier.

Three models have been used to analyze the obtained experimental data. The first is the Kerner's model,[19] which assumes no interaction between the blend components and is given by:

$$\frac{E_b}{E_o} = \text{RYM} = 1 + \left(\frac{\phi}{1 - \phi}\right)\left(\frac{15(1 - \upsilon)}{(8 - 10\upsilon)}\right) \tag{7}$$

In eq. (7), E_b and E_O are the tensile modulus of the nanoblends and that of the CAP–chitosan blend without NC, respectively.

The theoretical values obtained from eq. (7) are also plotted in Figure 4(b). The experimental data does not match with the predicted values indicating the existence of interaction between the blend components. The model for improved matrix–filler interaction is described by the Halpin–Tsai model given below in eq. (8).

$$\text{RYM} = \frac{1 + \eta_m\phi}{1 - \eta_m\phi} \tag{8}$$

where η_m is given by:

$$\eta_m = \frac{R_m - 1}{R_m + G} \tag{9}$$

In eq. (9), R_m is the ratio of filler modulus to matrix modulus. R_m was determined by trial and error to match with the experimental results as described earlier and was found to be 0.004. The values determined using eq. (8) is also plotted in Figure 4(b). The predicted values are closer to the experimental data and the trend also matches with that obtained experimental results.

The third model is the one developed by Sato and Furukawa,[21] which includes an adhesion parameter ξ, which varies from 0 to 1 for perfect adhesion to no adhesion. The model is described by eq. (10) below.

$$\mathrm{RYM} = \left[\left((1 + \frac{\phi^{2/3}}{2 - 2\phi^{1/3}}\right)(1 - \psi\xi) - \frac{\phi^{2/3}\psi\zeta}{\left(1 - \phi^{1/3}\right)\phi}\right] \tag{10}$$

where,

$$\psi = \left(\frac{\phi}{3}\right)\left(\frac{1 + \phi^{1/3} - \phi^{2/3}}{1 - \phi^{1/3} + \phi^{2/3}}\right) \tag{11}$$

The value of ξ was determined to match with the experimental results and has been found to be 0.7. The value of ξ indicates good adhesion and is between the two extremes. The theoretical data predicted using eq. (10) show a trend similar to that experimentally observed as shown in Figure 4(b).

Figure 4(c) shows a plot of REB versus volume fraction (ϕ) of NC. As observed earlier, there is a significant improvement in REB values by the addition of NC. Nielsen's model[23] has been used to analyze the observed values. The equation for this model is given below.

$$\mathrm{REB} = \frac{\epsilon_b}{\epsilon_o} = \left(1 - k\phi^{2/3}\right) \tag{12}$$

In eq. (12), ε_b and ε_O is the elongation at break for the nanoblends and that of the blend without NC, respectively. In eq. (12), k is an adjustable parameter, which depends on filler geometry. The value of k was computed by trial and error to get the best match for the obtained experimental results and this was found to be 0.09. The theoretical values plotted in Figure 4(c) do not match with the experimental values, which indicate that this model cannot explain the observed trend.

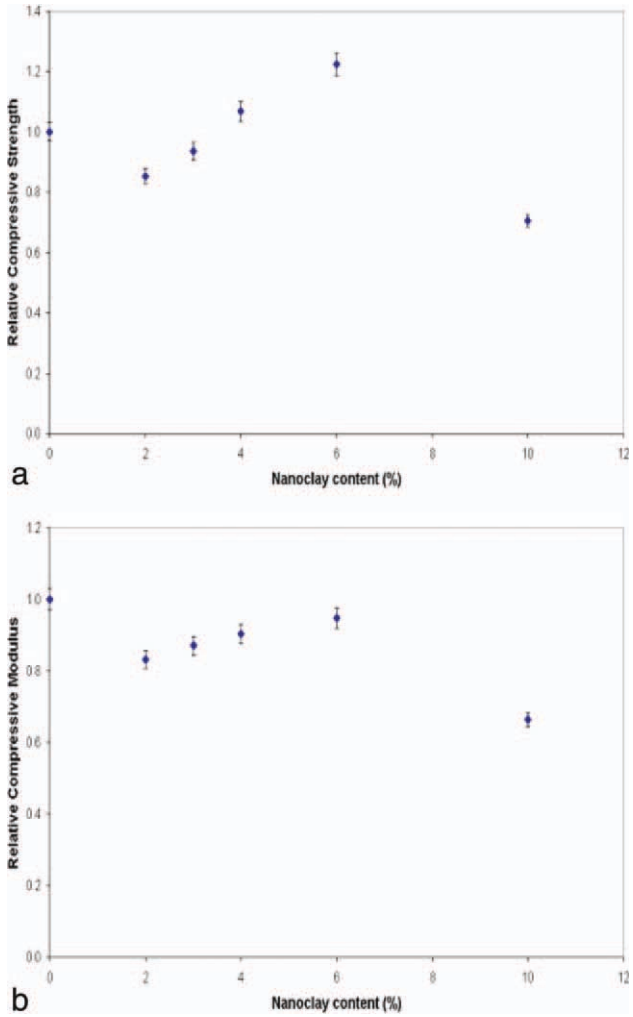

Figure 5 Variation of relative compressive properties with percentage nanoclay. (a) Relative compressive strength, (b) relative compressive modulus. [Color figure can be viewed in the online issue, which is available at wileyonlinelibrary.com.]

Compressive properties

Figure 5(a) shows a plot of relative compressive strength (RCS) of the blends versus percentage NC loading. The RCS value reaches an optimal value at 6% NC loading and the compressive strength of the blend increases by 22% (RCS = 1.22) when compared with blend without NC. The compressive strength of the blends reduce due to the addition of chitosan as it is brittle compared with CAP (the compressive strength of CAP is 12.96 Mpa). The nonlinearity of compressive properties has been discussed by Siqueira et al.[24] A threefold increase in compressive properties for biocompatible nanocomposites has been observed by Shi et al.[25]

Figure 5(b) shows the plot of relative compressive modulus (RCM) versus percentage NC loading for CAP–chitosan blends. The RCM values show a decreasing trend with the addition of functionalized

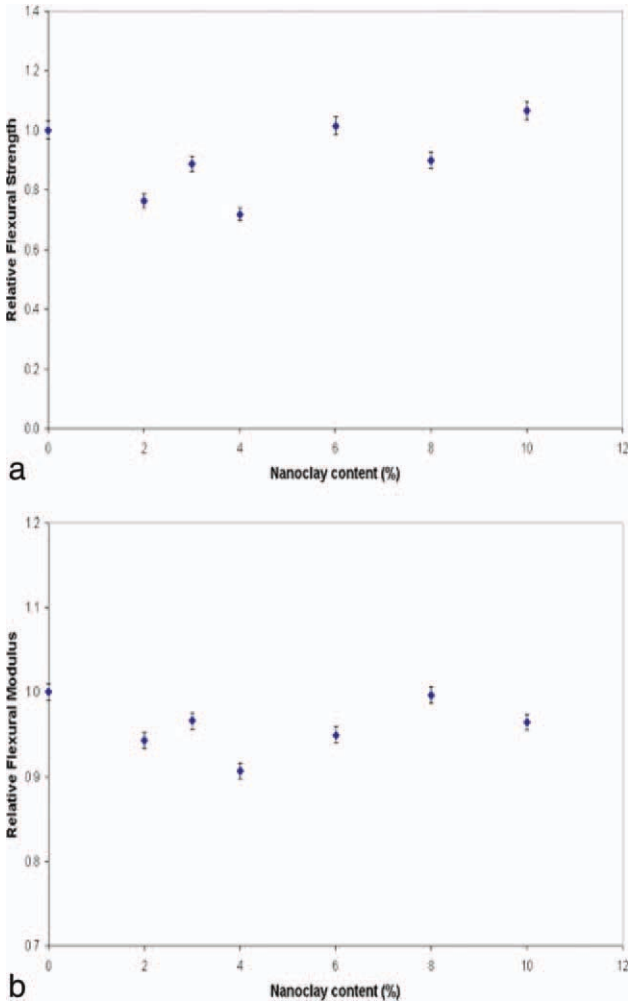

Figure 6 Variation of relative flexural properties with percentage nanoclay. (a) Relative flexural strength, (b) relative flexural modulus. [Color figure can be viewed in the online issue, which is available at wileyonlinelibrary.com.]

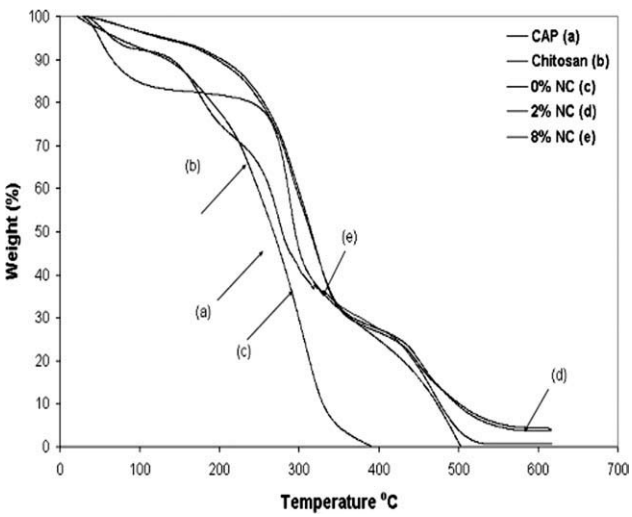

Figure 7 TGA themograms of pure CAP, chitosan, CAP–chitosan–nanoclay blends.

NC. The RCM values slightly reduce from 1.0 (without NC) to 0.947 with 6% NC as the optimal value. The plasticizing effect of ester group also plays a role in the reduction of modulus values as esters behave like internal plasticizers.[26]

Flexural properties

Figure 6(a) shows the relative flexural strength (RFS) for the blends versus percentage NC loading. Addition of NC to the blend did not show any improvement of RFS values. The RFS value for blend with 3, 6, and 8% NC were, respectively, found to be 0.966, 0.95, and 0.996.

Figure 6(b) show the relative flexural modulus (RFM) versus %NC loading. The blend containing no NC has a RFM-value of 1.0, while an optimal value of 1.014 was observed with 6% NC. Thus, in

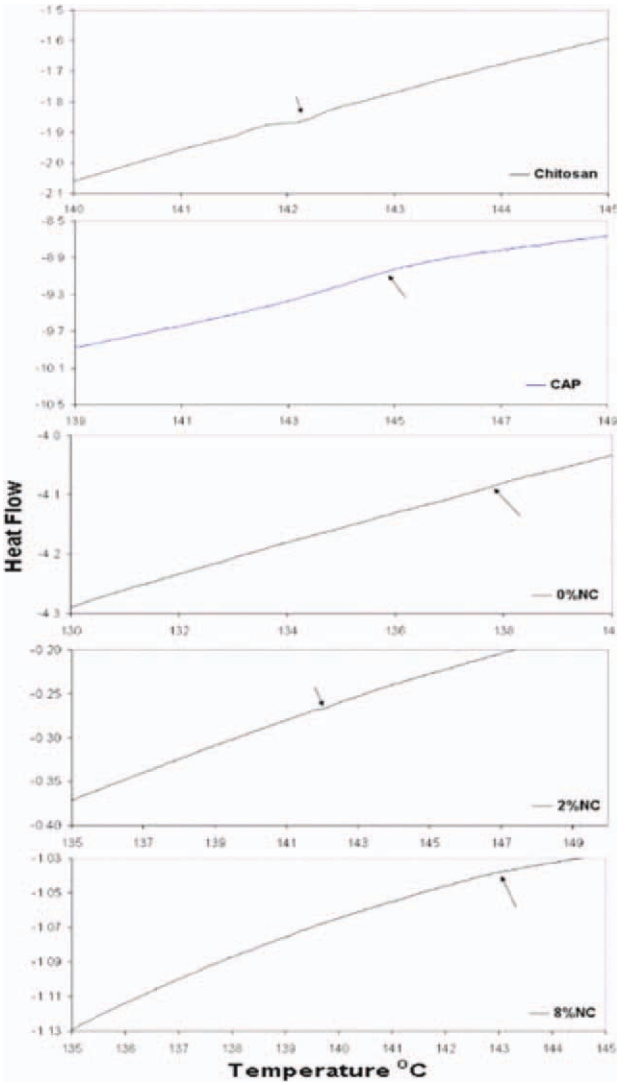

Figure 8 DSC thermograms for pure CAP, chitosan, CAP–chitosan–nanoclay blends. [Color figure can be viewed in the online issue, which is available at wileyonlinelibrary.com.]

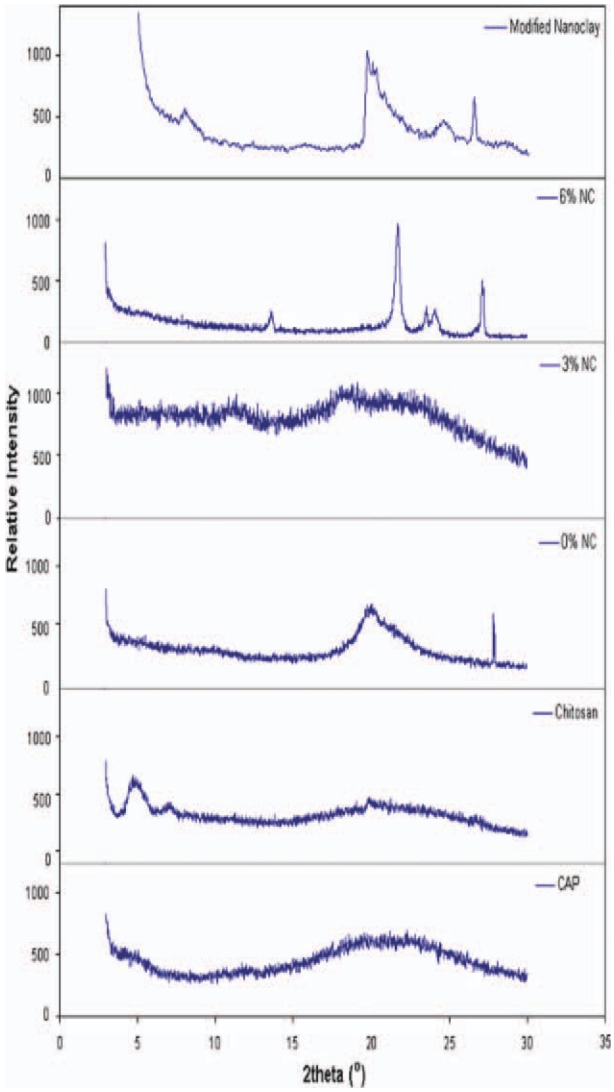

Figure 9 XRD spectra of pure CAP, chitosan, CAP–chitosan–nanoclay blends. [Color figure can be viewed in the online issue, which is available at wileyonlinelibrary.com.]

general, the flexural properties did not exhibit any improvement on NC addition. Sorrentino et al.[27] suggested that the enhancement of flexural properties is mainly due to the formation of three dimensional network of silicate layers. Similar observation for soy-based nanocomposites has been reported by Sithique et al.[28]

Thermogravimetric analysis

Figure 7 shows the TGA thermograms of CAP–chitosan blends. The thermograms for neat CAP, chitosan, and NC are also included in the figure for the sake of comparison.

Neat CAP [curve (a)] shows a main degradation peak at 310°C (with 78.1% weight loss) with a shoulder peak at 249°C (with 40.7% weight loss). At this temperature, elimination of acetyl and phthalyl groups takes place and the onset of backbone chain degradation takes place[29] and at 376°C, 99% weight loss occurs. Chitosan [curve (b)] undergoes a single stage degradation at 290.5°C (with 54.7% weight loss) owing to the degradation and deacetylation of chitosan.[30]

Among the CAP and chitosan, the latter has a better thermal stability probably owing to inter- and intramolecular hydrogen bonding. Similar observations have been reported by various authors.[31–33] The blends of CAP and chitosan [curve (c)] exhibit better interaction with only 47% weight loss at 310°C. Addition of NC slightly enhanced the thermal stability and an increase in char content was observed [curves (d) and (e)].

DSC thermograms

The DSC thermograms for CAP–chitosan blends are shown in Figure 8(a). Pure CAP shows a T_g at

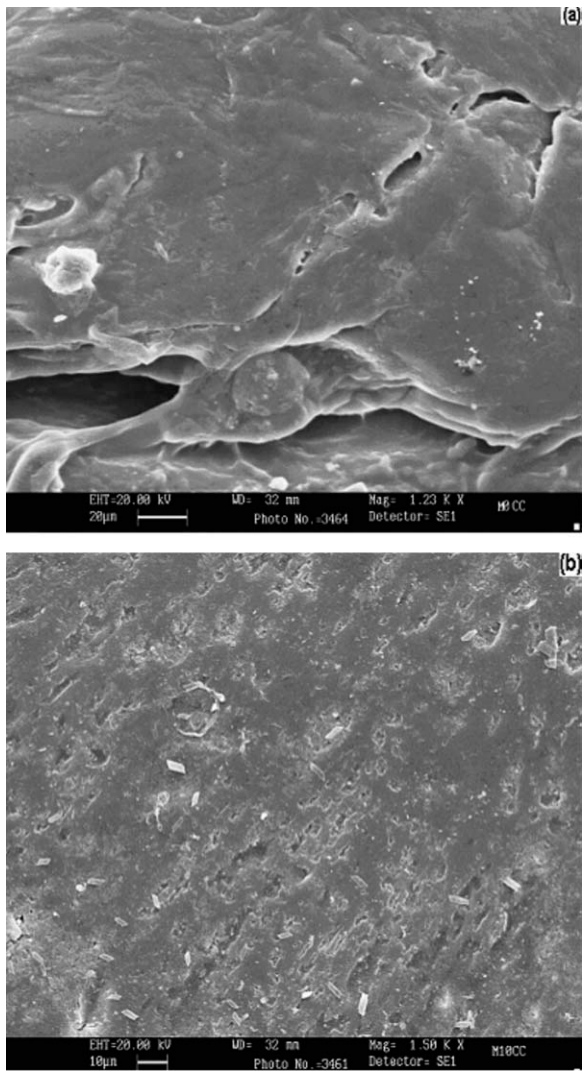

Figure 10 Scanning electron micrographs showing blend morphology for CAP–chitosan–NC. (a) CAP–chitosan blend without NC, (b) CAP–chitosan blend with 10% NC.

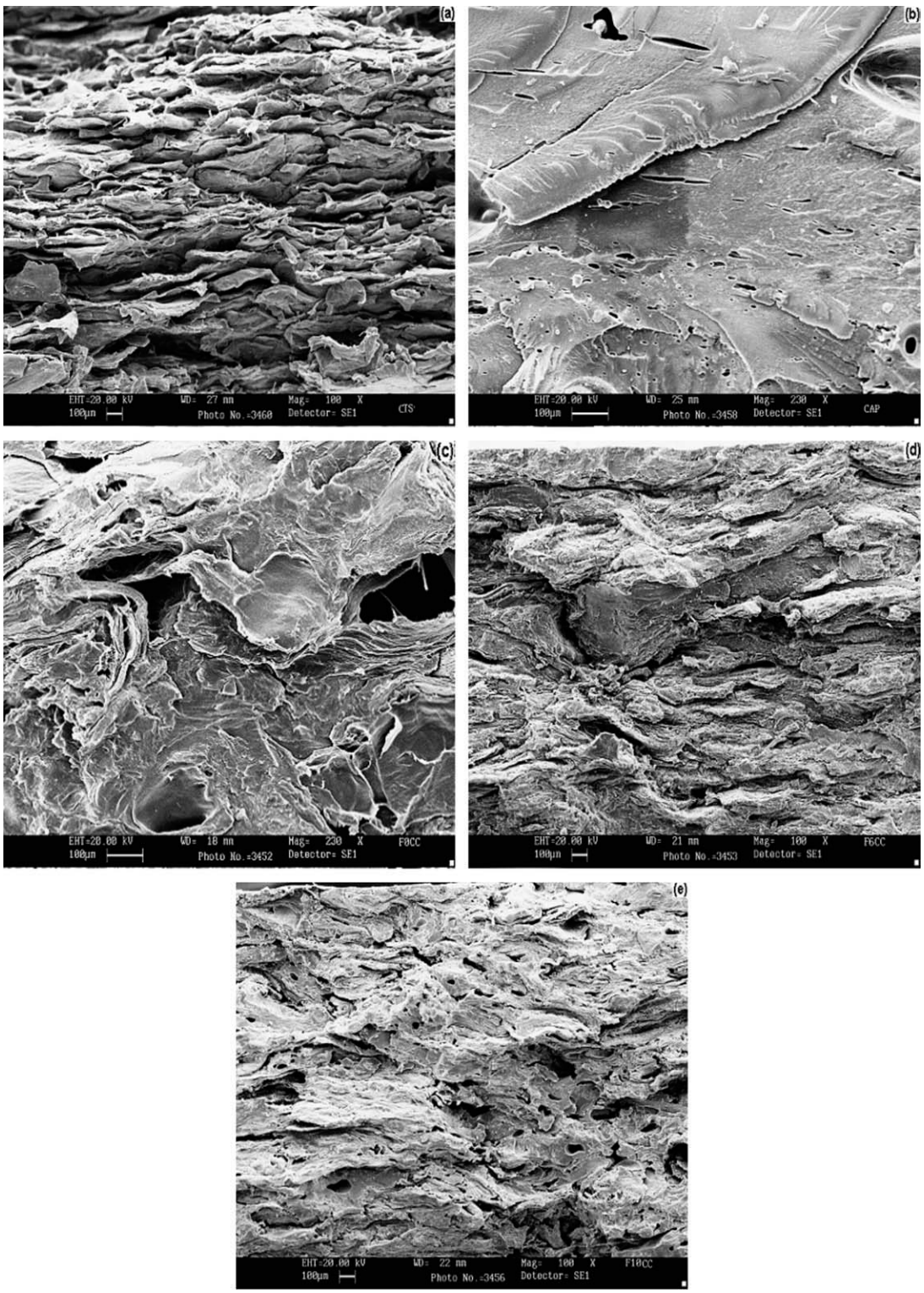

Figure 11 Scanning electron micrographs showing tensile fracture morphology for CAP–chitosan–NC. (a) Neat chitosan, (b) neat CAP, (c) CAP–chitosan blend without NC, (d) CAP–chitosan blend with 6% NC, (e) CAP–chitosan blend with 10% NC.

146°C. Similar observations have been reported by Rao et al.[34,35] The T_g of pure chitosan is at 142°C, which agrees with the results of Dong et al.[36] Another transition at 228°C may be attributed to liquid–liquid transition.[36] The composites without NC (0% NC) show a T_g at 140°C. Addition of 2 and 8% NC shows a T_g at 142.2 and 143°C, respectively. Thus, the T_g values for the blends are between the two extremes, i.e., between that of neat CAP and neat chitosan.

X-ray diffraction

The XRD patterns of CAP–chitosan biocomposites are shown in Figure 9. This figure also includes the XRD profiles for neat NC, CAP, and chitosan.

Neat NC indicates a characteristic diffraction at 2θ values of 8.03°, 19.778°, 24.73°, and 26.63°. Neat CAP has a main broad peak at a 2θ value of 22.038°, while that for chitosan the crystalline peak is at 20.792°. The blend of CAP and chitosan (without NC) has a peak at a 2θ value of 19.5574° accompanied by a small shoulder peak at 22°. The curve for blend loaded with 3% NC and 6% NC is also shown in Figure 9. The characteristic peak at 8.03° of NC is missing indicating that NC has formed an exfoliated structure with the blend components. Similar observation has been made for chitosan-based nanocomposites as reported by Wang and Wang.[37]

Blend morphology

Figure 10 shows the blend morphology of CAP–chitosan blend. The samples were etched in acid solution for 3 h so that the chitosan phase is removed. Figure 10(a) shows the morphology of CAP–chitosan blends. The morphology shows a highly deformed matrix as CAP and chitosan form partially miscible blends. It also includes a large number of elongated voids indicating resistance to removal of chitosan from the matrix. Figure 10(b) shows the morphology for blends containing 10% NC. The surface shows a large number of elongated voids caused by the debonded particles spread through the entire surface area. The elongated voids indicate deformation of the matrix and hence the resistance for removal of particles. Thus, the modified NC has dispersed uniformly in the entire surface.

Figure 11(a)–(e) shows the tensile fracture morphology of CAP–chitosan blends using SEM. Figure 11(a) shows the fractured SEM micrograph of neat chitosan. The micrograph shows a dense homogeneous structure with brittle characteristics, while that for CAP [Figure 11(b)] shows a sheared matrix with elongated voids due to tearing which indicates higher ductility when compared with chitosan. The blend without NC [Figure 11(c)] shows brittle failure characterized by sheared matrix accompanied by cavities left by debonded particles indicating the interactions between CAP and chitosan. Similar observations for chitosan blends with cellulose ethers were reported by Yin et al.[8]

The SEM micrograph of the tensile fractured surface of the blend containing 6% NC is shown in [Figure 11(d)]. The micrograph shows a dense homogeneous interlocked surface with a large number of elongated voids left by debonded particles. The numbers of voids were found to increase at higher filler content as shown in Figure 11(e).

TABLE I
Variation of Water Uptake of Neat CAP, Chitosan, and CAP–Chitosan–NC blends

Sample NC (%)	Water absorption (%)
CAP	68.07
Chitosan	70.07
NC0	22.21
NC2	17.70
NC3	14.28
NC4	20.27
NC6	23.52
NC8	19.49
NC10	22.86

Water uptake

Table I shows the values of water absorption characteristics of CAP–chitosan blends. chitosan and CAP have similar water uptake characteristics (i.e., 70.07 and 68.07%, respectively). The blends (with no NC) have a water uptake of 22.21%. This may be due to the interactions between CAP and chitosan, which form a network. The addition of NC up to 3% further reduces water absorbance as clay acts as a mechanical barrier. Addition of NC has further improved the water barrier properties owing to the tortuous path taken by the fluid and water absorption further drops down to 14.28%. However, at higher content of NC (>4%), the water absorbency increases. This may be due to the interaction between the excess amine groups on the NC surface with CAP and chitosan leading to a polymeric network. A similar observation was made by Zhang et al.,[38] in which case the surface groups of the clay-like material interacted with modified chitosan leading to an increase in water absorbency.

Biodegradation studies

Figure 12 shows the plot of percentage weight loss versus number of days for the CAP–chitosan blends. Chitosan is more biodegradable than CAP as the hydroxyl groups in the latter are replaced by ester groups. The blends show a retarded degradation for the first 3 days but, thereafter, the biodegradation is higher than either CAP or chitosan as observed in the first 30 days. The addition of NC further lowers the biodegradation up to 4% NC loading. This may be due to the interaction between CAP and chitosan with the amine groups of modified NC, which restricts the segmental motion at the interface causing the effective path length and diffusion time to increase. A similar observation has been made by Rindusit et al.[39] for methylcellulose–montmorillonite (MMT) composites.

However, beyond 4% NC, the blend exhibits a higher degradation than for lower NC loadings. The addition of increased modified NC induced large

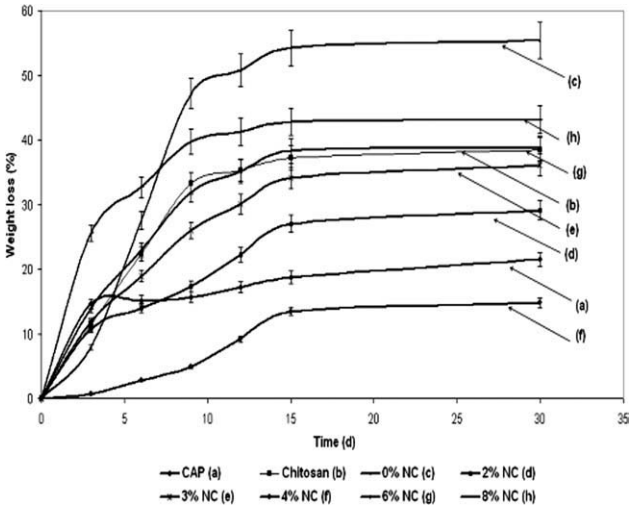

Figure 12 Biodegradation: variation of percentage weight loss with number of days for CAP–chitosan–NC blends.

amorphous regions and these regions are easily accessible during the degradation process. A similar observation was made by Wu and Wu,[40] when the biodegradation rates increased with 6% MMT when compared with 3% MMT loading.

Further, there is an interrelation between water uptake and degradability as higher water uptake accelerates the degradation process. Thus, increase in hydrophilicity increase leads to an increase in biodegradability. Thus, for water uptake, the blends loaded with lower content of NC show a lower uptake while blends loaded with >4% NC show increased water absorption characteristics and hence higher biodegradability.

CONCLUSIONS

CAP has been blended with chitosan along with modified NC as reinforcing filler. The mechanical and thermal properties were examined for NC variation. The tensile strength reached an optimal value with 6% NC. The tensile modulus reduces as NC loading increases, while the elongation at break increases. Theoretical models used to analyze the obtained experimental values indicated interactions between the blend components. Compressive strength improved by 22% by the addition of NC, while the flexural properties were unaffected for the nanocomposites. Addition of NC enhanced the thermal stability as indicated by an increase in char content. XRD studies revealed exfoliation of NC in the blend. Water uptake reduced to 14.28% on adding NC to the blends.

The authors thank the Department of Science and Technology (DST) for the financial assistance for carrying out this work under the Green Chemistry Programme (2007–2010).

References

1. Angles, M. N.; Dufresne A. Macromolecules 2008, 33, 8344.
2. Li, Q.; Zhou, J.; Zhang, L. J Polym Sci B Polym Phys 2009, 47, 1069.
3. El-Tahlawy, K.; Hudson, S. M.; Hebeish, A. A. J Appl Polym Sci 2007, 105, 2801.
4. El-Tahlawy, K.; Abdelhaleem, E.; Hudson, S. M.; Hebeish, A. J Appl Polym Sci 2007, 104, 727.
5. Hasegawa, M.; Isogai, A.; Onabe, F.; Usuda, M.; Atalla, R. H. J Appl Polym Sci 1995, 45, 1873.
6. Cai, Z.; Kim, J. J Appl Polym Sci 2009, 114, 280.
7. Altinisik, A.; Seki, Y.; Yurdakoc, K. Polym Compos 2009, 30, 1035.
8. Yin, J.; Lao, K.; Chen, X.; Khutoryanspiy, V. V. Carbohydr Polym 2006, 63, 238.
9. Liu, C.; Bai, R. J Membr Sci 2005, 267, 68.
10. Shih, C.; Shieh, Y.; Twn, Y. Carbohydr Polym 2009, 79, 169.
11. Wibowo, A. C.; Misra, M.; Park, H. M.; Drzal, R. S.; Mohanty, A. K. Compos A Appl Sci Manuf 2006, 37, 1428.
12. Huang, J.; Zhang, L.; Wang, X. J Appl Polym Sci 2003, 89, 1685.
13. Goswami, T. H.; Maiti, M. M. Polym Degrad Stabil 1998, 61, 335.
14. Shanmugharaj, A. M.; Rhee, K. Y.; Ryu, S. H. J Colloid Interface Sci 2006, 298, 854.
15. Menjoge, A. R.; Kulkarni, M. G. Int J Pharm 2007, 343, 106.
16. Balakrishnan, S.; Start, P. R.; Raghavan, D.; Hudson, S. D. Polymer 2005, 46, 11255.
17. Sue, H. J.; Gam, K. T.; Bestaoul, N.; Suprr, N.; Clearfield, A. Chem Mater 2004, 16, 242.
18. Sailaja, R. R. N.; Chanda, M. J. Appl Polym Sci 2001, 80, 863.
19. Willett, J. L. J Appl Polym Sci 1994, 54, 1685.
20. Bliznakov, E. D.; White, C. C.; Shaw, M. T. J Appl Polym Sci 2000, 77, 3220.
21. Hsieh, C. L.; Tuan, W. H. Mater Sci Eng 2005, 396, 202.
22. Zou, Y.; Wang, L.; Zhang, H.; Qian, Z.; Mou, L.; Wang, J.; Liu, X. Polym Degrad Stabil 2007, 83, 87.
23. Isabella, F.; Micheline, B.; Alain, M. Polymer 1998, 39, 4773.
24. Siqueira, G.; Bras, J.; Dufresne, A. Polymer 2010, 2, 728.
25. Shi, X.; Hudson, J. L.; Spicer, P. P.; Tour, J. M.; Krishnamoorti, R.; Mikos, G. Biomacromolecules 2006, 7, 2237.
26. Sagar, A. D.; Merrill, E. W. J Appl Polym Sci 1995, 58, 1647.
27. Sorrentino, A.; Gorasi, G.; Vittoria, V. Trends Food Sci Technol 2007, 18, 84.
28. Sithique, M. A.; Alagar, M.; Ali Khan. F. L.; Nazeer, K. P. Malays Polym J 2011, 6, 1.
29. Tserki, V.; Matzinos, P.; Koppon, S.; Panayiotou, C. Compos A 2005, 36, 965.
30. Tserki, V.; Matzinos, M.; Panayiotou, C. Compos A 2006, 37, 1231.
31. El-Hefian, E. A.; Naset, M. M.; Yahaya, A. H. J Chem 2010, 7, 1212.
32. He, L.; Xue, R.; Yang, D.; Liu, Y.; Song, R. Chin J Polym Sci 2009, 27, 501.
33. Duan, W.; Chen, C.; Jiang, L.; Li, G. H. Carbohydr Polym 2008, 73, 582.
34. Rao, V.; Ashokan, P. V.; Shridhar, M. H. J Appl Polym Sci 2000, 76, 859.
35. Rao, V.; Ashokan, P. V.; Amar, J. V. J Appl Polym Sci 2002, 86, 1702.
36. Dong, Y.; Rwan, Y.; Wang, H.; Zhao, Y.; Bi, D. J Appl Polym Sci 2004, 93, 1553.
37. Wang, L.; Wang, A. J Hazard Mater 2007, 147, 979.
38. Zhang, J.; Wang, Q.; Wang, A. Carbohydr Polym 2007, 68, 367.
39. Rindusit, S.; Jingjid, S.; Damrongsappul, S.; Tiptikaporn, S.; Tapeichi, T. Carbohydr Polym 2008, 72, 444.
40. Wu, T.; Wu, C. Polym Degrad Stabil 2006, 91, 2198.